Journal of Electroceramics (2021) 47:51–59
https://doi.org/10.1007/s10832-021-00259-2

Sensitive electrochemical detection of 4-nitrophenol through Copper doped CeO_2 nanoparticles

Anees A. Ansari[1] · **Manawwer Alam**[2]

Received: 28 February 2021 / Accepted: 21 July 2021 / Published online: 28 August 2021

Abstract

In this study, we developed an electrochemical sensor for sensitive detection of 4-NP in solution by using polyol-assisted co-precipitation process prepared copper doped cerium oxide nanoparticles (CeO_2:Cu NPs). Phase purity, crystal structure, and morphology of the as-prepared nanoproduct were examined by X-ray diffraction and transmission electron microscopy images. Chemical composition was determined by energy dispersive x-ray analysis(EDX). UV/Visible spectrum was measured to determine the optical absorption properties and bandgap energies of the material. The prepared CeO_2:Cu NPs were pasted on a glassy carbon electrode(GCE) to measure the electro-catalytic performance and further examining their sensing application through determining the 4-nitrophenol (4-NP) concentrations. The performance of the constructed electrode was assessed by cyclic voltammetry(CV) and electrochemical impedance spectroscopic(EIS) methods. The Cu doped CeO_2 NPs exhibited demonstrated excellent electrochemical performance in the presence of 4-NPs in a 10 pH phosphate buffer solution (PBS). The voltammetry-acquired kinetic evidence shows that 4NP electro-oxidation is a strictly diffusion-controlled process and that four electrons are involved in the reaction mechanism. The constructed CeO_2:Cu/GCE illustrated a high linearity range from 7.18-5000μL, a good detection limit (7.18 μL), with high sensitivity 1.4 μA $mmol^{-1}$ L. The reproducibility of the fabricated electrode was also monitored through nine consecutive CV cycles to measure their stability.

Keywords Cerium oxide · Copper · Nitrophenol · Impedance · Sensing

1 Introduction

Currently, pharmaceutical, chemical, and various polymeric and dye manufacturing units release various harmful materials [1, 2]. These manufacturing unit wastes are a severe threat to the ecosystem because they generated hazardous gases and pollute the water system and atmosphere [3–5]. Furthermore, industrial effluents are highly toxic and produced various diseases in human beings. Various organic effluents that discharge from various chemical industries are phenol, formaldehyde, hydrazine, catechol, bisphenol, and nitrophenol, etc [4, 6, 7]. Among these organic and industrial wastes, 4-nitrophenol(4-NP) has been subjected of much interest because of its hazardous nature, and produce various cancerous disease in human being. Consequently, the hazardous nature of 4-NP is an urgent need to identify its discharge from the industries or convert it into useful chemicals [5, 8–10]. Therefore, the development of a sensitive and selective detection device for 4NP is essential to prevent environmental pollution. Now a day's various techniques such as high-performance liquid chromatography, and UV/visible spectrophotometer has been utilizing for the detection of hazardous materials. But these techniques have some drawbacks, cost-effective, low sensitivity, selectivity, and complicated detection method, and high detection limit. These limitations of the currently utilized techniques draw attention to develop an alternate more reliable technique for sensitive and selective detection of hazardous substances. In the recent past, the electrochemical detection method is an alternative method for sensitive, selective, fast response, large detection range, eco-friendly, low cost, easy sample preparation, and produce reproducible results [11–15]. However, an important step is known to be the adjustment of the electrode surface in voltammetric tools to obtain a lower detection limit and to reduce the influence of interferents. In

✉ Anees A. Ansari
amustaqeemahmad@ksu.edu.sa; aneesaansari@gmail.com

[1] King Abdullah Institute for Nanotechnology, King Saud University, Riyadh 11451, Saudi Arabia

[2] Department of Chemistry, King Saud University, Riyadh 11451, Saudi Arabia

the past decade, different kinds of nanomaterials such as polyaniline nanofibers, chitosan, poly-thiophene, graphene, graphene oxide, quantum dots, plasmonic nanoparticles(NPs), metal NPs, and semiconductor metal oxides have been used for electrochemical sensing applications [16–20]. In terms of electrochemical electrode fabrication and their use in sensing applications, most of them suffer poor thermal, mechanical stability(polymers), high cost (Au, Ag), and limited electron transfer rate. Among them, semiconductor metal oxides are a unique class of materials because of their high thermal & mechanical stability, cost-effective, fast charge transfer rate, high isoelectric point, biocompatible, non-toxic, and high transparency in the visible region. Among the semiconductor metal oxides, n-type semiconductor cerium oxide(CeO_2) has been deliberated to be one of the most favorable metal oxide [11, 12, 15, 21, 22], owing to its novel physiochemical characteristics such as high thermal, mechanical stability, high isoelectric point (~9.2), large bandgap(3.4 eV), specific surface area, reversible oxidation state, high ionic mobility(conductivity), economic, eco-friendly, biocompatible and non-toxic [23–25]. It is a known fact that the CeO_2 has the ability to absorbed and release the oxygen species and these oxygen vacancies play a crucial role in the overall electro-catalytic performance of the electrochemical devices [26]. The reversible oxidation state of CeO_2 in between Ce^{3+} and Ce^{4+} relies on the O_2 partial pressure in the nearby atmosphere due to the valence state [27, 28]. This special property of CeO_2 has shown high thermochemical stability and large movement of oxygen vacancies and thus demonstrates enhanced efficiency in a redox reaction. So far its catalytic performance is mainly dependent on redox behavior and its high oxygen storage capability [29]. Although their oxygen storage capability can be altered by modification in crystal structure such as chemical composition, the evolution of surface defects, imbalance of oxygen species, specific surface area, the preferential introduction of reactive sides and structural impurities originate oxygen vacancies [30, 31]. These are the main important factors to improve the catalytic performance of CeO_2 crystal lattice. So that, monitoring these factors to enhancing the catalytic capabilities of CeO_2 is the main approach. To achieve the high catalytic activity, the preparation of ceria-based materials such as solid solutions, compound oxides, transition metal-ions substitution in the ceria crystal lattice is an effective technique. As a new area of importance, transition ion substitution in ceria matrix with selective elements, which can deform the lattice structure and create oxygen vacancies by removing Ce^{4+} ions, is a newly emerging field in catalytic applications. As reported in the literature, nickel ion-doped ceria is recorded to display superior catalytic reactivity of CO oxidization in comparison to the pure phase ceria, with complete conversion shifting down to 150° C [30, 32]. Due to their high catalytic performance against CO oxidation, which would be promising in potential applications in the reduction of automobile emissions, Cu ion substituted CeO_2 NPs or CuO-CeO_2 nanocomposites have received interest [33, 34]. Our research group have been synthesized and observed enhanced redox property measured through temperature program reduction/oxidation techniques in transition metal ion substituted CeO_2 crystal lattice [23, 24, 35, 36]. So that doping of transition metal ions in ceria crystal lattice is a versatile strategy to improve the redox activity of the as-prepared ceria NPs. Inspired from these strategies, we tried to doped Cu ion in CeO_2 crystal lattice for the construction of electro-catalytic host materials. Besides that, CeO_2 redox activity through the mobility of oxygen vacancies can be greatly improved/promoted, which is generated by doping of Cu ions into the crystal lattice, in which Cu ion distort/imbalance the lattice and enhanced ionic conductivity.

In this study, we prepared Cu-doped CeO_2 NPs through a polyol-based co-precipitation process for the construction of an electrochemical sensor. As-synthesized nanoproduct was characterized by X-ray diffraction(XRD), transmission electron microscopy (TEM), energy dispersive x-ray (EDX), UV/Visible absorption spectra, and redox properties through cyclic voltammetry (CV) and electrochemical impedance spectroscopic (EIS) techniques. An electrode was fabricated by deposition of CeO_2:Cu NPs on a glassy carbon electrode (GCE) for measuring the electrochemical characteristics and further determining their sensing application. The ability of the as-constructed CeO_2:Cu/GCE was then monitored using CV with varying 4-NP concentrations to assess the redox performance that had occurred.

2 Experimental

2.1 Materials

$Ce(NO_3)_36H_2O$ (99.9% BDH chemicals, UK), $Cu(NO_3)_2xH_2O$, ethylene glycol, NH_4OH, and C_2H_5OH were analytical grade and used directly as received from the procuring company. Milli-Q (Millipore, Bedford, USA) water was used for the synthesis and characterizations of the samples.

2.2 Synthesis

Briefly, for the synthesis of copper doped cerium oxide nanoparticles(CeO_2:Cu), 2 M molar solutions of cerium nitrate and copper nitrate were prepared separately in aqueous media. 9.4 ml of 2 M aqueous solution of cerium nitrate was mixed in 50 ml ethylene glycol and heated on the hotplate with constant magnetic stirring. Then 0.6 ml freshly prepared copper nitrate solution was slowly introduced in the ongoing reaction. The reaction was proceeding for 2 h

on the hot plate at 80 °C with magnetic stirring for homogeneous mixing. Later ammonia solution was added dropwise in the ongoing reaction for hydrolysis to get precipitation. Ethylene glycol form metal was used for complexation with cerium nitrate metal oxide, which decomposed slowly in the presence of ammonia solution. An appeared grey color precipitate was separated by centrifugation. Occurred precipitate was washed several times with Milli-Q water to remove unreacted reactants and dried at room temperature [15, 37–39]. Then this precipitate was dried in the oven at 400 °C for complete conversion into metal oxide. An obtained product was used for further characterization and their applications.

2.3 Characterization

X-ray diffraction (Rigaku, Dmax-2500 diffractometer) equipped with Cu *K*α as a radiation x-ray source. Field-emission Transmission electron microscopy (FE-TEM, JEM-2100F, JEOL, Japan) images along with energy dispersive x-ray(EDX) analysis were obtained to analyze the morphological structure and chemical composition of the product. The optical absorption spectrum was measured from UV/visible spectrophotometer (Agilent Technologies, USA) within the UV/Visible range from 200–800 nm wavelength. The electrochemical analysis was carried out by a three-electrode system by using an electrochemical analyzer (Metrohm Autolab, PGSTAT30, Switzerland). The three electrodes are linked to the electrochemical analyzer to build the sensor to complete the cell circuit in which the glassy carbon electrode (GCE) acts as a working electrode, Ag/AgCl (saturated KCl) acts as a reference, and the Pt foil acts as a counter electrode. The CeO_2:Cu NPs electrodes were produced under ambient conditions and were not stored in a cooled or inert atmosphere before testing the cyclic voltammetry(CV) results.

3 Results and discussion

3.1 Crystal structure and morphological study

XRD pattern was used for sample characterization of phase purity, crystal structure, the crystallinity of the as-prepared nanoproduct. XRD pattern in Fig. 1 demonstrated well-resolved reflection planes at 2θ 28.78, 33.35, 47.80, 56.59, and 59.39 values which are assigned to the (111), (200), (220), (311), and (222) reflection planes. These representative XRD diffraction planes are well-matched with the pure phase of CeO_2 cubic fluorite structure (space group: *Fm3m*; JCPDS card No. 0797) [11, 12, 22, 38, 39]. XRD data shows a strong alignment with

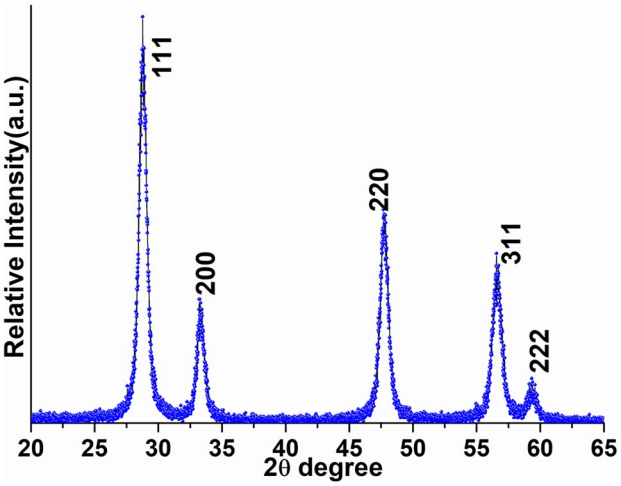

Fig. 1 X-ray diffraction pattern of CeO_2:Cu NPs

the literature studies as the peak locations and intensities of the reflection planes are completely match with the published literature reports [23, 35, 40–43]. The large diffraction peaks reflect that the prepared products are of high crystallinity in small grain sizes. The lack of impurity peaks of Cu ions is suggested that the doped ions are homogeneously distributed within the CeO_2 crystal lattices or its quantity is limited to the number of compounds to be identified by XRD. On doping, the composition of Cu ions-doped CeO_2 remains the same, suggesting the development of homogeneous Ce-Cu–O stable solutions. The average grain size of the nano product was measured from the full-width half maxima of the highly dominated reflection (111) plan observed at 28.78 2θ, and the crystalline size according to the Scherer equation is to be 11.5 nm.

Figure 2 illustrates the typical morphological structure of the as-prepared nanoproduct as analyzing from TEM photographs. TEM micrographs revealed the shape and size of the as-synthesized CeO_2:Cu NPs. The low-resolution TEM micrograph in Fig. 2(a) demonstrated the presence of high crystalline nature, rough surface, well-dispersed, irregular spherical shape with highly aggregated NPs and the size is ranging from 10–12 nm, which is in accord with the obtained XRD observations. To examine the phase purity, and crystallographic structure selected region electron diffraction analysis (SAED) was conducted as shown in Fig. 2(b, c). It can be found that most of them have lattice fringes with distances of around 0.3 nm that assigned to the well prominent (111) lattice plane of a cubic structure identical to fluorite. The Fig. 2(d) revealing four large rings with d-spacing of approximately 0.31, 0.27 and 0.22 nm, which could be due to (111), (200), (220) and (311) reflections of

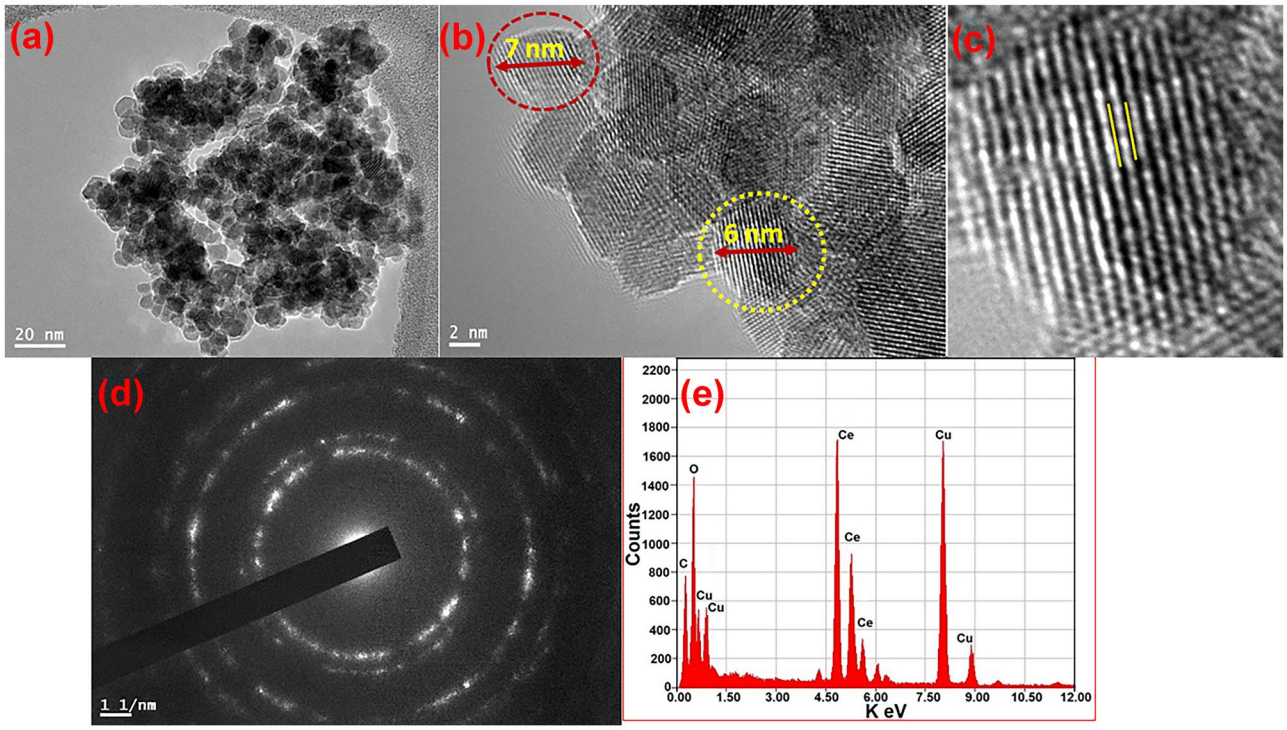

Fig. 2 Field-emission transmission electron microscopic images (**a**) low resolution FETEM image (**b**) high magnifying image shows the lattice fringes (**c**) high magnifying lattice fringes image and (**d**) selected area electron diffraction pattern (**e**) EDX analysis of the as-prepared CeO_2:Cu NPs

the CeO_2 cubic fluorite phase, respectively [23, 36, 42]. An enlargement in the reflection rings means that the NPs are tiny and/or have poly-crystallinity. Moreover, it revealed that the NPs are crystallized and the XRD peaks are very well balanced by diffraction rings. The findings of the TEM picture show that the Cu-doped CeO_2 NPs are exceptionally porous and are ideal for electro-catalytic use. The chemical composition of the as-prepared nano-product was determined from energy dispersive x-ray analysis(EDX). The EDX spectrum in Fig. 2(e) illustrates all peaks related to the Ce, O, and Cu ions. The spectrum is also shown well dominant signals of Cu and C, which belong to the carbon-coated Cu grid.

3.2 Optical properties

The optical absorption spectrum of CeO_2:Cu NPs was obtained from UV/visible spectrophotometer to determine the optical properties of the nanoproduct. Because ceria is shown strong absorption in the visible region so that it also can be used as an indicator to examine the existence or formation of cerium oxide NPs (Fig. 3(a)) [23, 35,

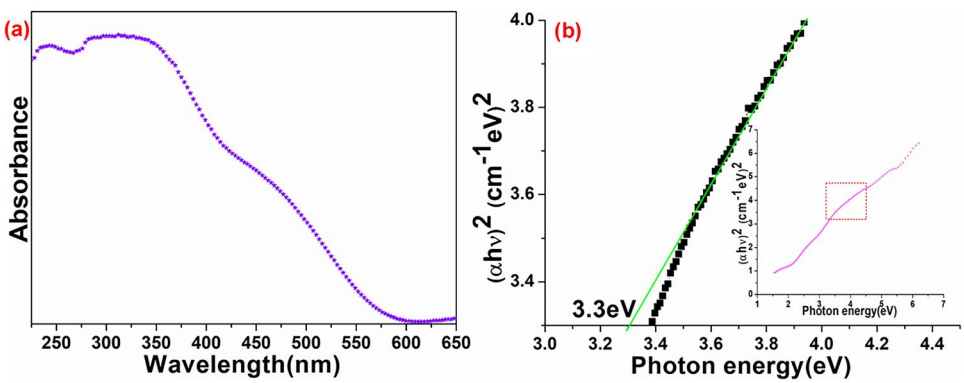

Fig. 3 (**a**) UV/Vis absorption spectrum of CeO_2:Cu NPs and (**b**) Energy band gap, photon energy ($h\nu$) vs $(\alpha hv)^2$

36, 42]. So that strong absorption in the visible region strongly validated the existence of CeO_2 NPs. The energy band gap value was estimated from the absorption spectrum according to the Schuster-Kubelka–Munk formule [44–48]. An effective energy bandgap(E_g) was observed 3.3 eV (Fig. 3(b)) [23, 35–39, 42].

3.3 Electrochemical characterization

The electrochemical performance of the as-synthesized nano-product was evaluated by the three-electrode cell configuration method. Figure 4(a) illustrates the cyclic voltammetry of the as-designed electrode concerning the blank glassy carbon electrode (GCE)electrode and bare electrode in 4-nitrophenol solution in the potential range from -1.75 to 1.75 V at a scan rate 50 mV/s. The bare GCE electrode does not show any redox behavior in phosphate buffer solution (PBS; 0.1 M, pH 7.2). Similarly, bare electrode in the presence of 4-NP does not show any oxidation–reduction band as shown in Fig. 4(a). It suggested that the bare electrode is free from the redox reaction so that it does not show any redox phenomenon even in 4-NP. But a significant enhancement in anodic and cathodic peak current was appeared in CeO_2:Cu NPs modified GCE electrode in the presence of 4-NP. An observed alteration in CeO_2:Cu NPs modified electrode redox peaks indicate that the NPs support the electron communication process over the surface-modified GCE electrode. Furthermore, the CeO_2:Cu/GCE efficiently electro-catalyze through oxidation of the analyte (4-NP) and provide an electrochemical signal in the presence of PBS. In that case, copper doped ceria film is responsible for fast electron transfer in the electrochemical reactions.

To examine the electron transfer kinetics and potentiality of the modified electrode, the modified CeO_2:Cu/GCE electrode was scan at different potentials (0.005- 0.15 mV/s) in PBS solution as represented in Fig. 4(b). As observed in

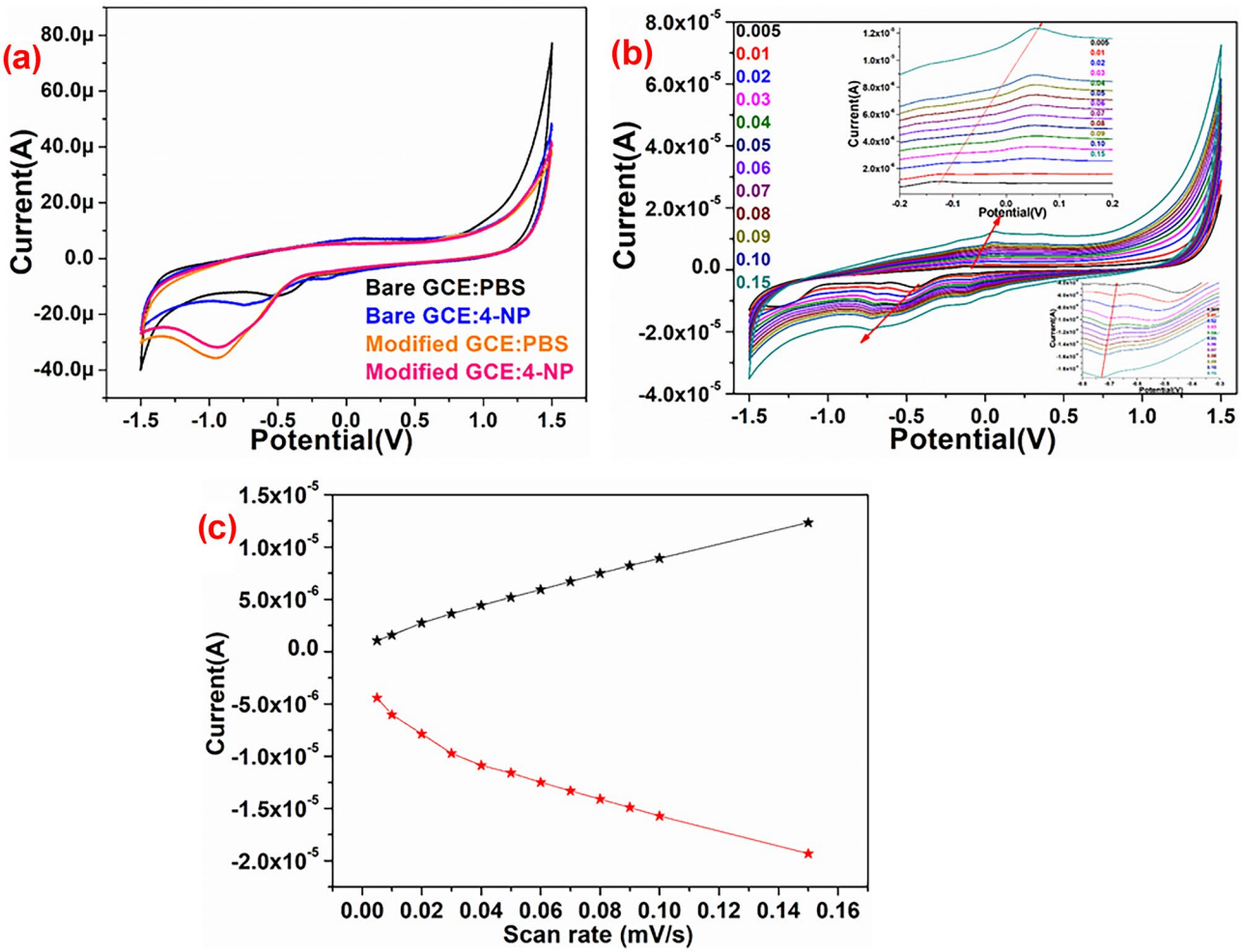

Fig. 4 **(a)** Cyclic voltammograms of bare and modified electrodes in the absence and presence of 4-NP (500 μM) in 0.01M phosphate buffer (pH 7.4) at 100 mVs^{-1}scan rate (**b&c**). CV of CeO_2:Cu/GCE electrode as a function of scan rate (5, 10, 20, 30, 40, 50, 60, 70, 80, 90, 100 and 150 mV) in ascending order in PBS solution

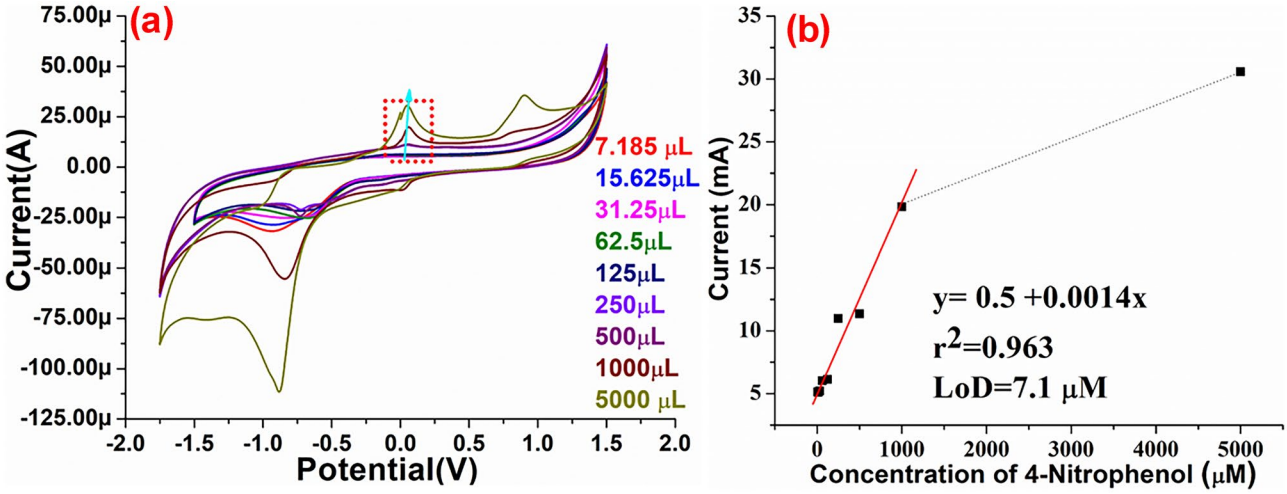

Fig. 5 **(a)** Electrochemical responses of CeO_2:Cu/GCE electrode at different concentrations of 4-NP in 0.01M phosphate buffer (**b**) linearity sensitivity curve observed from CeO_2:Cu/GCE electrode between 4-NP concentration and current

Fig. 4(b), the redox potential (anodic/cathodic) was gradually increased on increasing the scan potential rate along with shifting peak maxima. The measured spectra revealed the correlation between the current and the increase in the capacity of the 4-NP sensor manufactured. In the spectra, small reduction and oxidation peaks were witnessed denoting a low potential; but, when the potential was raised, improvements were seen in the spectra to both redox peaks, the CeO_2:Cu/GCE may be more susceptible to 4-NP detection through applying increasing voltage. It endorsed that the redox mechanism has been carried out and CeO_2:Cu NPs electrode support in fast electron communication over the surface of electrode which is diffused well-organized and quasi-reversible process [14, 49, 50] (Fig. 4(c)).

3.4 Sensing properties

The fabricated CeO_2:Cu/GCE electrode was further used to examine the electrochemical performance as a function of various concentrations of 4-NPs (7.185-5000µL) at a constant potential (100 mV) in PBS solution. As represented in Fig. 5(a) a chronological variation in redox peaks was observed in the CV spectra on the addition of 4-NPs concentrations in the potential range from -2.0- + 2.0 V. Moreover, with the rise in 4-NP quantity, the linear increase in oxidation peaks. As shown in Fig. 5(a, b) the magnitude of the current is closely associated with the 4-NP quantity at the oxidative/ reduction peak, increasing as the concentration of 4-NP rises. It also implies that with the improvement in 4-NP quantity, the current arising from ion movement increases, resembling the fast transfer of electrons to the conduction band. It showed that, because of the diffusion-controlled mechanism, the CeO_2:Cu/GCE electrode successfully catalyzes the electrochemical oxidation of 4-NP. The calibration graph of 4-NP concentration versus peak current maxima achieved is shown in Fig. 5(a, b), while the sensing parameters of the CV spectra experimentally measured are shown in Fig. 5(b). The fabricated electrochemical electrode shows two detection ranges such as 7.81–125 and 125–5000 µL with the slope value of 0.5 µA/µM. The fabricated electrode is sensitive to the 4-NP concentration of 7.18 µM (LOD) as determined by this curve. The regression coefficient at a higher concertation scale is observed to be high in respect to a lower one. The sensing performance of the fabricated electrode was further examined by the electrochemical impedance spectroscopy method at different concentration range (7.81–5000 µL). EIS is an effective technique to measure the electron transfer rate over the modified and unmodified GCE. The cole–cole plot diameter gives the charge transfer resistance, such as the obstacle delivered by the electrode material to the transfer of charge from the solution to the electrode that can be associated with the surface change [50, 51]. The curve found at greater frequencies, refers to the process of electron communication rate, while the rectilinear portion is typical of the lesser frequency spectra and reflects the procedure of diffusion-limited electron communication. As observed in Fig. 6 the semicircle curve is gradually reduced on increasing the 4-NP concentrations. It illustrates that the charge transfer rate is sequentially improving on the addition of 4-NP concentration, resulting in semicircle shape is gradually suppressed [11, 12, 22]. These results

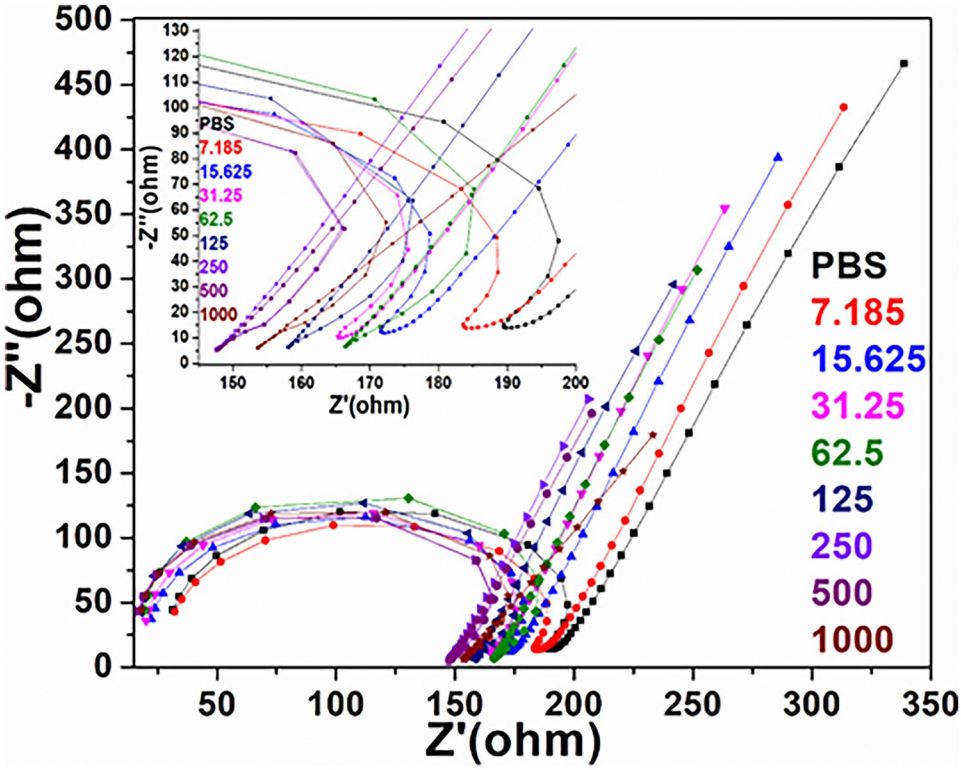

Fig. 6 Electrochemical impedance responses of CeO_2:Cu/GCE electrode at different concentrations of 4-NP in 0.01M phosphate buffer (inset shows the high magnifying figure)

are in good agreement with the cyclic voltammetry sensing observations.

3.5 Electrochemical stability & reproducibility

For a successful sensing device stability and reproducibility of the fabricated electrode is an important parameter. To examine the stability of the fabricated CeO_2:Cu/GCE electrode was monitored through cyclic voltammetry at a constant potential at nine consecutive cycles in the presence of PBS and 4-NP solutions. Figure 7(a) demonstrates the electrochemical performance of the fabricated electrode. As exhibited in Fig. 7(b) fabricated electrodes illustrate the excellent stability performance at nine successive cycles, resulting it can produce suitably reproducible results. These findings revealed that because of its excellent durability and reproducible performance, the produced CeO_2:Cu/GCE sensing electrode is highly appreciable for generating the sensing results.

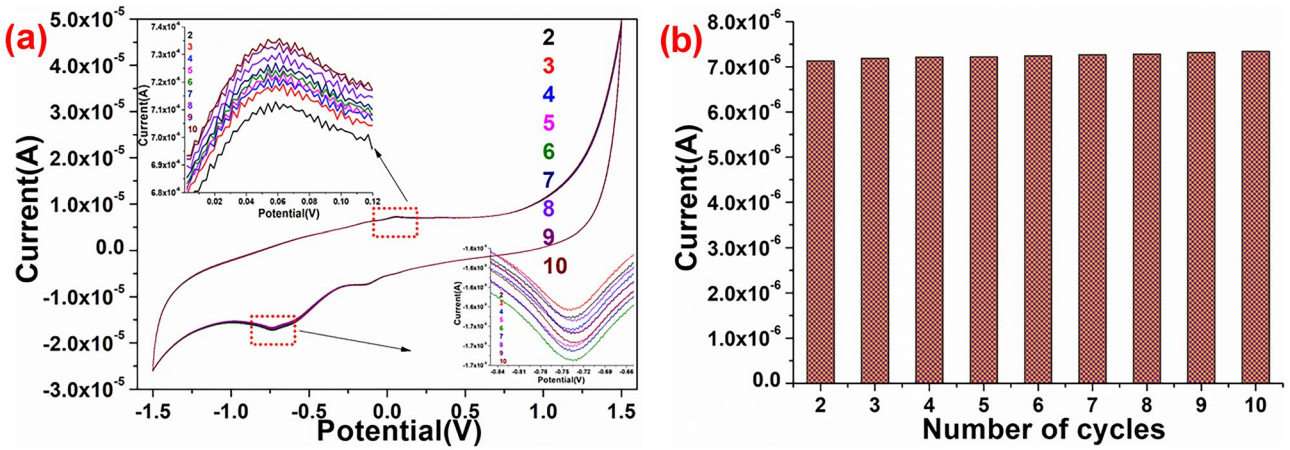

Fig. 7 **(a, b)** Electrochemical reproducibility measured by CV at nine consecutive cycles of CeO_2:Cu/GCE electrode in presence of 500 µM (4-NP) in 0.01 M PBS at 100 mV/s **(c)** Stability test first and after 35 days at the same conditions

4 Conclusions

The polyol-assisted co-precipitation synthesis process was employed to prepare the CeO_2:Cu NPs. XRD results verified the phase purity, crystal structure, and crystallinity of the nano-product. Tem micrographs exhibited the irregular spherical, rough shape, and highly aggregated NPs. EDX analysis shows the presence of copper ions in the ceria crystal lattice. Optical absorption spectra and energy bandgap values also verified the formation of pure phase CeO_2 NPs. The electrochemical performance of the nano-product was evaluated by CV, it illustrates the excellent electro-catalytic nature of the product. The increase in redox magnitude of CeO_2:Cu NPs modified electrode may be attributed due to the Cu-ion doping in ceria lattice that enhances the ionic mobility within the crystal lattice, resulting in an increase in the electron transportation rate over the electrode surface. As observed in cyclic voltammetry data, doping of Cu ions contributes to higher oxidation potential and accelerate the transition of oxygen vacancies by further oxygen species, the electro-catalytic efficiency of the fabricated electrode is increased. The fabricated electrochemical sensor shows excellent characteristics to sensitive detection of 4-NP such as sensitivity 1.4 μA $mmol^{-1}$ L, low detection limit (7.18μL), linear range (7.18–5000 μL), and long term stability of the electrode. This observed finding suggests that the CeO_2:Cu NPs is a promising substance that can experimentally be utilized for sensitive detection of hazardous chemical or electro-catalytic devices for catalysts.

Acknowledgements The authors extend their sincere appreciation to the Deanship of Scientific Research at King Saud University for funding this Research Group (RG-1439-089).

Data availability All data generated or analysed during this study are included in this published article.

Declarations

Conflict of interest The authors declare that there are no conflicts of interest.

References

1. J.K. Jung, K.K. Alam, M.S. Verosloff, D.A. Capdevila, M. Desmau, P.R. Clauer, J.W. Lee, P.Q. Nguyen, P.A. Pastén, S.J. Matiasek, J.F. Gaillard, D.P. Giedroc, J.J. Collins, J.B. Lucks, Nat. Biotechnol. **38**(12), 1451–1459 (2020)
2. K.M. Emran, S.M. Ali, H.E. Alanazi, J. Electroanal. Chem. **856**, 113661 (2020)
3. W. Wang, H.J. Li, M.Y. Yin, K.W. Wang, Q.L. Deng, S. Wang, Y.K. Zhang, Sens. Actuators B Chem. **255**, 1422–1429 (2018)
4. Z. Xiong, H. Zhang, W. Zhang, B. Lai, G. Yao, Chem. Eng. J. **359**, 13–31 (2019)
5. X. Zhang, G. Ren, M. Li, W. Yang, Q. Pan, Cryst. Growth Des. **19**(11), 6308–6314 (2019)
6. V. Anbumannan, M. Dinesh, R.T. Rajendra Kumar, K. Suresh, Ceram. Int. **45**(17,Part B), 23097–23103 (2019)
7. P. Balasubramanian, T.S.T. Balamurugan, S.M. Chen, T.W. Chen, J. Hazard. Mater. **361**, 123–133 (2019)
8. W.C. Pan, S.H. Zhang, F. He, S.L. Gai, Y.B. Sun, P.P. Yang, Cryst. Eng. Comm. **17**(30), 5744–5750 (2015)
9. Y. Liu, Y. Liu, Z. Liu, F. Du, G. Qin, G. Li, X. Hu, Z. Xu, Z. Cai, J. Hazard. Mater. **368**, 358–364 (2019)
10. M.M. Rahman, T.A. Sheikh, A.M. Asiri, K.A. Alamry, M.A. Hasnat, Anal. Methods **12**(27), 3470–3483 (2020)
11. A.A. Ansari, A. Kaushik, P.R. Solanki, B.D. Malhotra, Electrochem. Commun. **10**(9), 1246–1249 (2008)
12. A.A. Ansari, P.R. Solanki, B.D. Malhotra, Appl. Phys. Lett. **92**(26), 263901 (2008)
13. P. R. Solanki, A. Kaushik, A.A. Ansari, B.D. Malhotra, Appl. Phys. Lett. **94**(14), 143901 (2009)
14. A.A. Ansari, A. Kaushik, P.R. Solanki, B.D. Malhotra, Electroanalysis **21**(8), 965–972 (2009)
15. A. Kaushik, P.R. Solanki, A.A Ansari, S. Ahmad, B.D. Malhotra, Nanotechnology **20**(5), 055105 (2009)
16. A. Friggeri, F.C.J.M. van Veggel, D.N. Reinhoudt, R.P.H. Kooyman, Langmuir **14**(19), 5457–5463 (1998)
17. M.M. Rahman, A. Wahid, M.M. Alam, A.M. Asiri, Mater. Today Commun. **16**, 307–313 (2018)
18. L.T. Liu, R.N. Hua, B.J. Chen, X.H. Qi, W. Zhang, X. Zhang, Z.L. Liu, T. Ding, S. Yang, S. T.Y. Zhang, L.H. Cheng, Nanotechnology **30**(37), 375703 (2019)
19. A.F. Mulaba-Bafubiandi, H. Karimi-Maleh, F. Karimi, M. Rezapour, J. Mol. Liq. **285**, 430–435 (2019)
20. N. Ahmad, A.S. Al-Fatesh, R. Wahab, M. Alam, A.H. Fakeeha, J. Mater. Sci.: Mater. Electron. **31**(14), 11927–11937 (2020)
21. P.R. Solanki, C. Dhand, A. Kaushik, A.A. Ansari, K.N. Sood, B.D. Malhotra, Sens. Actuators B Chem. **141**(2), 551–556 (2009)
22. A.A. Ansari, P.R. Solanki, B.D. Malhotra, J. Biotechnol. **142**(2), 179–184 (2009)
23. A.A. Ansari, J.P. Labis, M. Alam, S.M. Ramay, N. Ahmad, A. Mahmood, Acta Metal. Sin.-Engl. Lett. **29**(3), 265–273 (2016)
24. A.A. Ansari, J.P. Labis, M. Alam, S.M. Ramay, N. Ahmed, A. Mahmood, Anal. Lett. **50**(8), 1360–1371 (2017)
25. A.A Ansari, N. Ahmad, M. Alam, S.F. Adil, S.M. Ramay, A. Albadri, A. Ahmad, A.M. Al-Enizi, B.F. Alrayes, M.E. Assal, A.A. Alwarthan, Sci. Rep. **9**, 7747 (2019)
26. Z.L. Wang, G.R. Li, Y.N. Ou, Z.P. Feng, D.L. Qu, Y.X. Tong, J. Phys. Chem. C **115**(2), 351–356 (2011)
27. H. Xu, A.L. Wang, Y.X. Tong, G.R. Li, ACS Catal. **6**(8), 5198–5206 (2016)
28. J.X. Feng, S.H. Ye, H. Xu, Y.X. Tong, G.R. Li, Adv. Mater. **28**(23), 4698–4703 (2016)
29. H. Yen, Y. Seo, S. Kaliaguine, F. Kleitz, Angew. Chem. **124**(48), 12198–12201 (2012)
30. X. Zhang, J. Wei, H. Yang, X. Liu, W. Liu, C. Zhang, Y. Yang, Eur. J. Inorg. Chem. **2013**(25), 4443–4449 (2013)
31. D. Wang, Y. Kang, V. Doan-Nguyen, J. Chen, R. Küngas, N.L. Wieder, K. Bakhmutsky, R.J. Gorte, C.B. Murray, Angew. Chem. Int. Ed. **50**(19), 4378–4381 (2011)
32. T. Li, G. Xiang, J. Zhuang, X. Wang, Chem. Commun. **47**(21), 6060–6062 (2011)
33. S.L. Zhong, L.F. Zhang, L. Wang, W.X. Huang, C.M. Fan, A.W. Xu, The Journal of Physical Chemistry C **116**(24), 13127–13132 (2012)
34. X. Xie, Y. Li, Z.Q. Liu, M. Haruta, W. Shen, Nature **458**(7239), 746–749 (2009)
35. A.A. Ansari, J. Labis, M. Alam, S.M. Ramay, N. Ahmad, A. Mahmood, J. Chin. Chem. Soc. **62**(10), 925–932 (2015)

36. A.A. Ansari, J. Labis, M. Alam, S.M. Ramay, N. Ahmad, A. Mahmood, Phase Transit. **89**(3), 261–272 (2016)
37. A.A. Ansari, A. Kaushik, J. Semicond. **31**(3), 033001 (2010)
38. A.A. Ansari, J. Semicond. **31**(5), 053001 (2010)
39. A.A. Ansari, S.P. Singh, B.D. Malhotra, J. Alloy. Compd. **509**(2), 262–265 (2011)
40. C.S.S. Pavan Kumar, R. Pandeeswari, B.G. Jeyaprakash, J. Alloy. Compd. **602**, 180–186 (2014)
41. F.A. Al-Agel, E. Al-Arfaj, A.A. Al-Ghamdi, Y. Losovyj, L.M. Bronstein, W.E. Mahmoud, J. Magn. Magn. Mater. **360**, 73–79 (2014)
42. A.A. Ansari, J. Labis, M. Alam, S.M. Ramay, N. Ahmad, A. Mahmood, J. Electroceram. **36**(1–4), 150–157 (2016)
43. A.A. Ansari, M. Alam, M.A. Ali, Colloids Surf. A: Physicochem. Eng. Asp. **613**, 126116 (2021)
44. D.E. Zhang, X.J. Zhang, X.M. Ni, J.M. Song, H.G. Zheng, Chemphyschem. **7**(12), 2468–2470 (2006)
45. Z. Wang, Z. Quan, J. Lin, Inorg. Chem. **46**(13), 5237–5242 (2007)
46. S.A. Ansari, M.M. Khan, M.O. Ansari, S. Kalathil, J. Lee, M.H. Cho, RSC Adv. **4**(32), 16782–16791 (2014)
47. D. Channei, B. Inceesungvorn, N. Wetchakun, S. Phanichphant, A. Nakaruk, P. Koshy, C.C. Sorrell, Ceram. Int. **39**(3), 3129–3134 (2013)
48. D. Channei, B. Inceesungvorn, N. Wetchakun, S. Ukritnukun, A. Nattestad, J. Chen, S. Phanichphant, Sci. Rep. **4**(1), 5757 (2014)
49. A.A. Ansari, P.R. Solanki, B.D. Malhotra, Sens. Lett. **7**(1), 64–71 (2009)
50. A.A. Ansari, A. Kaushik, P.R. Solanki, B.D. Malhotra, Bioelectrochemistry **77**(2), 75–81 (2010)
51. A.A. Ansari, G. Sumana, M.K. Pandey, B.D. Malhotra, J. Mater. Res. **24**(5), 1667–1673 (2009)